ACS OMEGA

http://pubs.acs.org/journal/acsodf

Article

Mathematical Model for the Industrial SMTO Reactor with a SAPO-34 Catalyst

Hongbo Jiang,* Linzhi Yuan, Defei Li, and Yushi Chen

Cite This: *ACS Omega* 2023, 8, 9630−9643

Read Online

ACCESS | Metrics & More | Article Recommendations

ABSTRACT: The methanol-to-olefins (MTO) technology creates a new non-oil route to produce light olefins. This paper reports a 14-lump MTO kinetic model for SAPO-34 catalyst, combined with the hydrodynamic model for the fast fluidized bed reactor of the industrial SMTO process. Selective deactivation is considered to quantify the product selectivity and abrupt catalytic activity change. Moreover, referring to the parallel compartment (PC) model, the activity difference between the circulating spent catalyst and the regenerated catalyst is considered. The validation results with the optimized kinetic parameters showed good agreement between the calculated value and the actual value. Sensitivity analysis of the industrial SMTO process was performed. According to the results, the established mathematical model can provide guidance for industrial production operations.

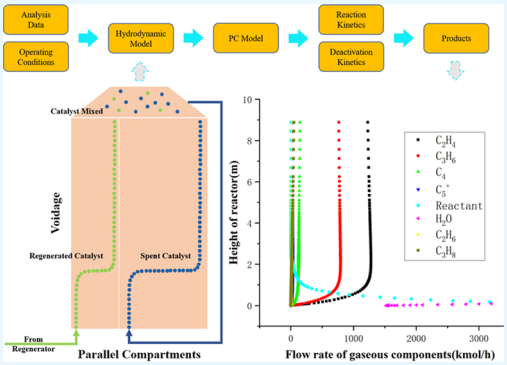

1. INTRODUCTION

Ethylene and propylene are the basic raw materials in the chemical industry.[1] The increasing demand for lower olefins requires new production routes besides steam cracking and fluid catalytic cracking, which account for around 90% of the world's olefin production.[2−5] The MTO technology creates a new route to produce light olefins.[6] The reactant methanol can be obtained from non-oil sources such as coal and natural gas, and CO_2 is also a potential feedstock to produce methanol.[7]

Since the discovery of the MTO reaction by Mobil researchers in 1977, several companies and research institutions, including ExxonMobil, UOP, Lurgi, Dalian Institute of Chemical Physics (DICP) and SINOPEC, have successfully brought MTO techniques into stream, respectively.[8−11] These methods achieve a methanol conversion of up to 99%, and the selectivity of ethylene and propylene could reach up to 80% or even higher.

The excellent MTO performance of SAPO-34 zeolite was first reported by DICP in 1990.[12] SAPO-34 exhibits high catalytic activity due to the moderate acid strength, and its special 3D channels are found to be more shape-selective toward light olefins. Moreover, researchers demonstrated the good thermal stability and high-temperature steam stability of SAPO-34.[13] These factors ensure the long lifetime of the catalyst circulating between a high-temperature regenerator and a high-water-content reactor. Besides SAPO-34, ZSM-5 zeolite is also effective in the methanol conversion reaction applied to the methanol-to-propylene (MTP) process, showing strong acidity, high activity, high stability, and pronounced shape selectivity.[14]

Different acid densities and topological structures lead to different reaction mechanisms on these two kinds of catalysts. Most researchers adopted the hydrocarbon pool (HCP) theory[15−17] to explain the reaction mechanism on SAPO-34, while the reaction mechanism on ZSM-5 is consistent with the dual-cycle theory,[18,19] although recently some researchers applied the dual-cycle theory to the SAPO-34 catalyst.[20,21] According to the HCP theory, the HCP species are mainly polymethylated aromatic compounds formed in the early stage.[15] These trapped species act as cocatalysts through continuous methylation and dealkylation reactions, the latter producing mainly ethene and propylene. Furthermore, two distinct mechanistic pathways for methanol conversion and subsequent olefin dealkylation were suggested according to the HCP mechanism.[2] The side-chain mechanism proceeds via methanol methylation on polymethylbenzenium ions; then, one of the side chains of the aromatic compound continuously grows until it is dealkylated as olefin.[22−25] In contrast, in the paring mechanism, the growth of the aromatic compound causes complex structural rearrangements, which also lead to olefin release.[25] Otherwise, HCP species will be converted to coke with an increase in the reaction time, which has complicated impacts on the product yield.

Received: January 15, 2023
Accepted: February 22, 2023
Published: March 3, 2023

https://doi.org/10.1021/acsomega.3c00304
ACS Omega 2023, 8, 9630−9643

Table 1. List of Kinetic Models of the MTO Reaction

year	mechanism	researcher	catalyst	feature
1983	molecular-scale	Mihail[27]		involving 53 elementary reactions.
1995	lumped	Bos[28]	SAPO-34	8 lumps, 12 reactions. coke is considered as key component.
2000	lumped	Gayubo[29]	SAPO-34	neglecting effects of coke caused inaccuracy.
2001	molecular-scale	Park[30,31]	HZSM-5	the rate constants were obtained by the single-event method.
2004	molecular-scale	Alwahabi[32]	SAPO-34	the result was consistent with Park, except C_6^+.
2005	lumped	Qi[33,34]	SAPO-34	the influence of water is considered.
2007	lumped	Chen[35]	SAPO-34	methanol and dimethyl ether (DME) were treated as one lump.
2009	lumped	Hu[36,37]	SAPO-34	methane was lumped as a C_1 lump alone.
2014	molecular-scale	Sedighi[38]	SAPO-34	a simplified kinetic elementary reaction model was proposed.
2015	lumped	Ying[39−41]	SAPO-34	the kinetics of industrial DMTO reaction.
2016	lumped	Rostami[42]	SAPO-34	11 reactions and 13 species. the effect of coke was considered.

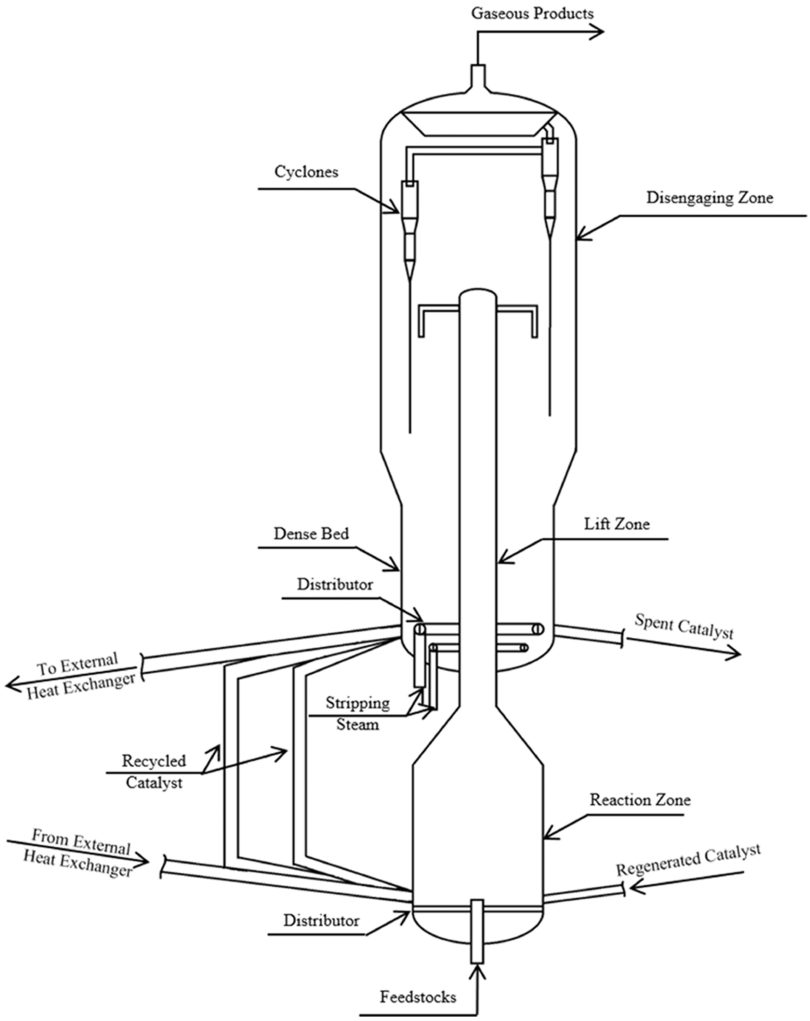

Figure 1. Schematic diagram of the SMTO reactor.

Kinetic modeling is an important tool for evaluating reaction kinetics, heat management, product distribution, and reactor performance.[26] Although methanol is the only reactive feed in the industrial MTO process, the reaction network is extremely large because of many different intermediates and byproducts, making the kinetic modeling of the MTO process challenging. There are primarily two types of kinetic models developed for the MTO process in the open literature. The molecular-scale model is to list all possible elementary reactions and estimate the kinetic parameters by experiment and quantum theory. This type of model provides detailed information about individual compounds; however, a lack of experimental data on reaction intermediates may result in a poor estimation of the kinetic parameters. The error and limited operating range of industrial data also bring difficulties. Calculation will be difficult if reactor mathematical models are combined with complex molecular-scale kinetic models. On the other hand, lumped models divide compounds into several lumps according to the principle of similar kinetic characteristics. As each lump is treated as a single component, the reaction network is much simplified. This method has been widely used in the simulation of various reactors and has great advantages.

https://doi.org/10.1021/acsomega.3c00304
ACS Omega 2023, 8, 9630−9643

Various kinetic models for the MTO reaction system have been reported in recent years, and some of them are presented in Table 1.

Methanol conversion and coke deposition are considerably fast in the MTO process and release a lot of heat at the same time. However, the coke content and reaction temperature have significant impacts on the reaction. To achieve the optimum coke content and remove reaction heat in time, a fluidized bed is preferred in the MTO process. Circulating fluidized beds are widely used in various modern industrial processes, such as fluid catalytic cracking and coal combustion. They have favorable hydrodynamics, reactions, and heat transfer characteristics due to their high gas−solid flow rate and intensive contact. Meanwhile, the spent catalyst can be continuously transferred to the regenerator to restore activity. Solids move concurrently upward with the gas in a fluidized bed reactor. The rate of distribution of solids in the fluidized bed reactor is different from that in the fixed bed reactor, and the gas−solid flow is heterogeneous. An increase in the gas flow rate or a decrease in the solid circulation rate usually leads to a slight decrease in the solid holdup. Kwauk,[43,44] Li,[45−49] Bai,[50,51] Grace,[52−54] Levenspiel, and Kunii[55] introduced the modeling of fluidized bed reactors. Turbulent fluidized beds and fast fluidized beds have been applied in the industrial MTO process. Few complete mathematical models have been applied to the industrial MTO process in the open literature, as their data were obtained from laboratories. Zheng[56] established a complete mathematical model, and the simulation results were in good agreement with the open pilot data of an MTO fluidized bed reactor.

Complete mathematical models for the industrial SMTO reactor were established, including the methanol reaction model, catalyst deactivation model, and hydrodynamic model of the fast fluidized bed. Industrial data were used to fit and validate the model parameters. Factors Influencing SMTO process are discussed in this paper, providing guidance for the simulation, analysis, and operation optimization of the industrial SMTO reactor.

2. DESCRIPTION OF TECHNOLOGY

The SMTO process is developed by the Shanghai Research Institute of Petrochemical Technology (SRIPT), Sinopec Co. Ltd. This process employs a fast fluidized bed reactor that can achieve 99.8% methanol conversion and more than 80% total olefin yield, and a regenerator is applied for continuous catalyst regeneration.

2.1. Overview of the Device. The geometry of the industrial SMTO reactor with a methanol feed of 1800 kt/a is shown in Figure 1. The reaction zone is 8.884 m high and 8.3 m wide (inner diameter), which is operated in the fast fluidization regime and equipped with an external heat exchanger to control the reaction temperature. The regenerated catalyst from the regenerator and spent catalyst from the dense bed with and without heat transfer are fed into the bottom of the reactor. The stream of feed (mainly methanol and steam) flows into the reaction zone through the distributor. Reactions take place when methanol comes in contact with the catalyst. The gaseous phase, including products and remaining reactants, rises and fluidizes the catalyst particles. Some of the catalysts fall along the wall of the reactor, while the others are carried into the upper disengaging zone via a riser with a smaller inner diameter. The gaseous products are released from the top outlet for further separation and purification, and the catalyst carried by the gas drops to the dense bed. To keep the activity of the MTO catalyst, part of the spent catalyst in the dense bed is transferred to the regenerator to maintain a relatively stable mean coke content. Most of the catalyst in the dense bed is transferred back to the bottom of the reactor to maintain the catalyst holdup. A small quantity of steam is fed to the dense bed to maintain the flowability of solids.

2.2. Catalyst. A new SMTO-2 catalyst is used in the production, and the crystallite, the density of the effective center, and the catalytic performance are improved compared with those of the SMTO-1 catalyst by the innovation of SRIPT. The results show that the selectivities of ethylene and propylene are significantly improved, the methanol unit consumption is decreased, and the application of the new catalyst has significant economic benefits. Table 2 shows the properties of the SMTO-2 catalyst.

Table 2. SMTO Catalyst Properties

projects	unit	indicators
shape		microspherical
skeleton density	kg/m^3	2100−2500
particle density	kg/m^3	1400−1700
stacking density	kg/m^3	690−810
pore volume	mL/g	0.18−0.28
specific surface area	m^2/g	190−270
specific heat	kJ/kg·°C	1
particle size composition		
<20 μm	vol %	1.0−2.0
20−40 μm	vol %	2.0−10.0
40−60 μm	vol %	20.0−25.0
60−80 μm	vol %	25.0−35.0
80−100 μm	vol %	20.0−25.0
>100 μm	vol %	15.0−20.0

2.3. Analysis Methods. Industrial data, including the catalyst coke content, temperature, pressure, and gaseous product composition, are collected from an industrial SMTO unit. Temperature and pressure are read and recorded directly from temperature and pressure gauges. The gaseous product composition is analyzed by a GC-MS system, and the catalyst coke content is measured by C744.

2.4. Operating Conditions. A total of 32 sets of data were used in modeling. The operation conditions of the MTO reactor are as follows: the methanol feed flow rate is 170−260 t/h, where the mass percentage of methanol is 94.5−96.0%, that of water is 3.8−5.0%, and that of high carbon hydrocarbons and higher alcohols is about 0.38%; the dilute steam is 0−30 t/h; the total feed includes methanol feed and dilute steam, and their mixing temperature is 185−200°C; the total circulation amount of the catalyst is 2500−4500 t/h, among which the regenerated catalyst from the regenerator constitutes 65−95 t/h at a temperature of 663−670 °C, the dense bed catalyst returning to the inlet of the reactor through the circulating inclined tube constitutes 2300−4000 t/h at a temperature of 470−480 °C, the dense bed catalyst returned to the inlet of the reactor through the external heat exchanger constitutes 100−500 t/h, and the temperature is 310−380 °C. The absolute pressure of the reaction inlet is 0.245−0.275 MPa, and the pressure difference of the feed distribution plate is 7−9 kPa.

https://doi.org/10.1021/acsomega.3c00304
ACS Omega 2023, 8, 9630−9643

3. REACTOR MODEL

3.1. Judgment of the Fluidized Bed Flow Pattern. Gas−solid fluidized beds can be operated in different hydrodynamic flow regimes such as fixed bed, delayed bubbling, bubbling, slugging, turbulent to fast fluidization, and pneumatic conveying.[57] Each stage has its own unique feature, and it is important to differentiate these flow regimes because hydrodynamics, mixing, heat and mass transfer behaviors, and reactor performance all vary from regime to regime. There is a characteristic transition velocity between the regimes.

Chen[58] proposed a method to estimate the formation of the fast fluidization regime. When the solid flow rate G_s is greater than the minimum solid flow rate G_{sm} and $u_c < u_g < u_{pt}$, it belongs to the fast fluidized bed. The calculation of u_{pt} refers to the research of Bi.[59] According to the result, the SMTO reactor is a fast fluidized bed within the industrial operating range.

3.2. Characteristics of the Fast Fluidized Bed. The methanol conversion reaction is rapid, with a large amount of heat released. To prevent the secondary reaction of ethylene and propylene as well as the further coke deposition on the catalyst, a quick separation of gas products and the catalyst is required. An ideal reactor for commercial MTO processes is the fast fluidized bed reactor, which is characterized by the disappearance of the dilute−dense interface, a bed density that is dilute in the upper zone and dense in the lower zone, good gas−solid contact, fast transfer rate, small gas−solid back-mixing, and high equipment utilization.

3.3. Fast Fluidized Bed Model Calculation. Hydrodynamic modeling is an important part of the reactor mathematical model. The coupling application of the reaction kinetic model and the hydrodynamic model can simulate and predict the profile of gas−solids systems, the distribution of products, and the influence of operating conditions. Li and Kwauk[48] first noticed that the axial distribution of particles in the fast fluidized bed usually presented an S-shaped profile. The top area is the dilute-phase zone, and the bottom area is the dense-phase zone. There is a transition zone between the dilute-phase and dense-phase zones and a turning point of the bed voidage distribution Z_i in the transition zone; the bed voidage distribution diagram is shown in Figure 2.

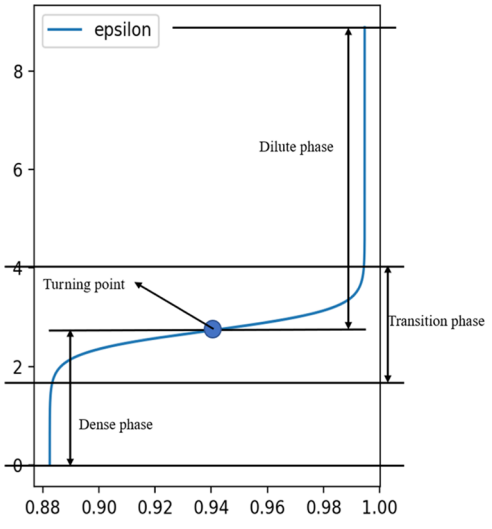

Figure 2. Profile of the fast fluidized bed.

The calculation of the axial bed voidage distribution for a fast fluidized bed adopts the four-parameter model proposed by Kwauk.[60]

$$\frac{\varepsilon - \varepsilon_d}{\varepsilon^* - \varepsilon} = \exp[-(z - Z_i)/Z_0] \tag{1}$$

Parameters involved can be obtained by the following equations

$$Z_0 = 500 \exp[-69(\varepsilon^* - \varepsilon_d)] \tag{2}$$

$$Z_i = \ln\left(\frac{(\varepsilon^* - \varepsilon_e)}{(\varepsilon^* - \varepsilon_d)}\right)/(-\gamma) \tag{3}$$

$$\varepsilon_d = 0.756Ra^{0.0741} \tag{4}$$

$$\varepsilon^* = 1 - \frac{G_s^*}{\rho_s(u_g - u_t)} \tag{5}$$

In eqs 2−5,

$$\varepsilon_e = 1 - \frac{G_s}{\rho_s(u_g - u_t)} \tag{6}$$

$$G_s = F_{cat}/(3600\ \Omega) \tag{7}$$

The calculation of G_s^* refers to Bai and Kato[61]

$$G_s^* = 0.125Fr^{1.85}Ar^{0.63}\left(\frac{\rho_s}{\rho_g} - 1\right)^{-0.44}\mu/d_p \tag{8}$$

$$Ar = \frac{gd_p{}^3\rho_g(\rho_s - \rho_g)}{\mu^2} \tag{9}$$

$$Fr = u_g/(9.91d_p)^{0.5} \tag{10}$$

$$Ra = (18Re_s + 2.7Re_s{}^{1.687})/Ar \tag{11}$$

$$Re_s = d_p\rho_g(u_g - u_d)/\mu \tag{12}$$

$$u_d = G_s/\rho_s \tag{13}$$

The calculation of γ refers to Adanez[62]

$$\gamma = (0.88 - 420d_p)/((u_g - u_t)^2D^{0.6}) \tag{14}$$

where u_t, the terminal particle velocity, is obtained by the following equations

$$u_t = Re_t\mu/(d_p\rho_g) \tag{15}$$

When $Ar < 18$

$$Re_t = Ar/18 \tag{16}$$

When $18 < Ar < 82\,500$

$$Re_t = \left(\frac{Ar}{7.5}\right)^{1/1.5} \tag{17}$$

When >82 500

$$Re_t = 1.74Ar^{0.5} \tag{18}$$

After the above parameters are confirmed, the axial distribution of the voidage along the height of the fast fluidized bed can be determined.

https://doi.org/10.1021/acsomega.3c00304
ACS Omega 2023, 8, 9630−9643

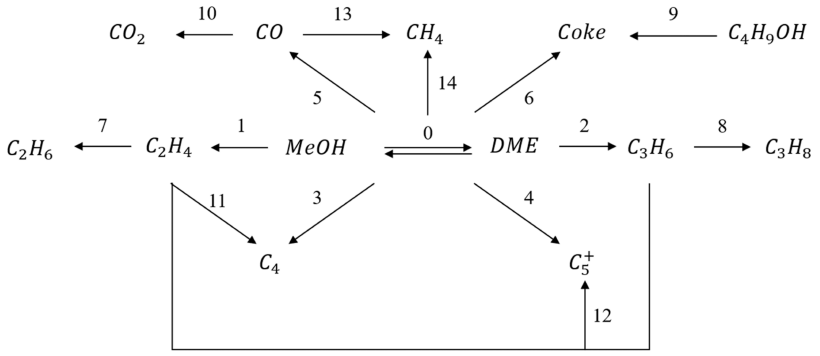

Figure 3. Kinetic scheme for the MTO reaction.

Table 3. Reactions and Kinetic Equations

no.	reaction type	reaction	kinetics equation
0		$CH_3OH \leftrightarrow 0.5CH_3OCH_3 + 0.5H_2O$	$r_0 = k_0P_{react}/H - k_0/K_0P_{DME}^{0.5}P_{H_2O}^{0.5}$ (19)
1		$CH_3OH = 1/2C_2H_4 + H_2O$	$r_1 = \phi_1k_1P_{react}/H$ (20)
2	main reactions	$CH_3OH = 1/3C_3H_6 + H_2O$	$r_2 = \phi_2k_2P_{react}/H$ (21)
3		$CH_3OH = 1/4C_4H_8 + H_2O$	$r_3 = \phi_3k_3P_{react}/H$ (22)
4		$CH_3OH = 1/5C_5H_{10} + H_2O$	$r_4 = \phi_4k_4P_{react}/H$ (23)
5		$CH_3OH = CO + 2H_2$	$r_5 = \phi_5k_5P_{react}/H$ (24)
6		$CH_3OH = coke + 0.65H_2 + H_2O$	$r_6 = \phi_6k_6P_{react}/H$ (25)
7		$C_2H_4 + H_2 = C_2H_6$	$r_7 = k_7P_{C_2H_4}P_{H_2}$ (26)
8		$C_3H_6 + H_2 = C_3H_8$	$r_8 = k_8P_{C_3H_6}P_{H_2}$ (27)
9		$C_4H_9OH = 4coke + 2.6H_2 + H_2O$	$r_9 = k_9P_{C_4H_9OH}$ (28)
10	side reactions	$CO + H_2O \leftrightarrow CO_2 + H_2$	$r_{10} = k_{10}P_{H_2O}P_{CO}$ (29)
11		$2C_2H_4 \leftrightarrow C_4H_8$	$r_{11} = k_{11}P_{C_2H_4}^2 - k_{11}/K_{11}P_{C_4H_8}$ (30)
12		$C_2H_4 + C_3H_6 \leftrightarrow C_5H_{10}$	$r_{12} = k_{12}P_{C_2H_4}P_{C_3H_6} - k_{12}/K_{12}P_{C_5H_{10}}$ (31)
13		$CO + 3H_2 \leftrightarrow CH_4 + H_2O$	$r_{13} = k_{13}P_{CO}P_{H_2}^3 - k_{13}/K_{13}P_{H_2O}P_{CH_4}$ (32)
14		$CH_3OCH_3 = CO + H_2 + CH_4$	$r_{14} = \phi_{14}k_{14}P_{react}/H$ (33)

4. KINETIC MODEL

4.1. MTO Reaction Mechanism over SAPO-34 Zeolite. The formation of C−C bonds from C_1 reactants has been debated in the past decades. Early research provided many direct pathway mechanisms to explain how the C−C bond originates from methanol or dimethyl (DME), including the carbene mechanism,[63−65] oxysonium ylide mechanism,[66,67] carbocation mechanism,[68,69] free radical mechanism,[70] etc. The generation of the first C−C bond has remained a contentious issue until now, so researchers turned to indirect pathways such as the HCP mechanism to describe the reaction process. According to the HCP mechanism on SAPO-34 zeolite proposed by Dahl and Kolboe,[15,16,71−73] methanol conversion reactions are parallel, which is widely accepted now.

4.2. MTO Reaction Network. We endeavored to develop a kinetic model for industrial application, so species obtained by daily industrial analysis were considered while lumping the MTO reaction system. Based on the HCP mechanism, a 14-lump kinetic network of the MTO process was proposed, as illustrated in Figure 3. It is possible to consider the intermediate species by applying the pseudo-steady-state approximation (PSSA)[74] to modelling MTO reaction system. However, intermediate species such as polymethylated aromatic compounds are not involved in the reaction network of our model as we obtained the data from an industrial unit, and no analysis data for intermediate comparisons are available. The network involved three reactant lumps, including methanol (MeOH), DME, and higher alcohols, and 11 product lumps, including CH_4, C_2H_6, C_2H_4, C_3H_6, C_3H_8, C_4, C_5^+, CO, CO_2, H_2, and coke. The following hypotheses were proposed for the kinetic model

(1) Methanol and DME rapidly reach equilibrium over the catalyst surface,[35,75−77] and a rapid enough reaction rate is given.
(2) Reactant conversion rate is related to the sum of methanol and DME concentration.
(3) C_4 and C_5^+ are represented as C_4H_8 and C_5H_{10}, respectively, in simulation, and higher alcohols are represented as C_4H_9OH.
(4) H_2O and H_2 are not shown in this parallel reaction network, but their effects are considered in rate laws.
(5) Higher alcohols are impurities in the feedstock, and they are only converted to coke.

https://doi.org/10.1021/acsomega.3c00304
ACS Omega 2023, 8, 9630−9643

(6) The C/H molar ratio of coke is 1/0.7.
(7) The feed and catalyst were assumed to mix instantaneously at the inlet of the fast fluidized bed.

The proposed reaction network for the MTO process is shown in Figure 3.

Although this reaction network has a limitation in expressing the autocatalytic feature of the MTO reaction related to the intermediate species, which is not included in the network, it has been widely accepted in a number of research cases.[39,35,76]

4.3. MTO Chemical Reactions and Kinetic Equations. The reactions included in the MTO process and the corresponding reaction kinetic equations are shown in Table 3:

The Arrhenius equation is used to reflect the effect of temperature on the reaction rate

$$k_i = k_{i0} \exp\left(-\frac{Ea_i}{RT}\right) \tag{34}$$

The water in the reaction system will be adsorbed on the active center of the catalyst. Therefore, a water adsorption resistance term H was introduced into the reaction rate equation to quantify the influence of water.[34]

$$H = 1 + K_w X_w \tag{35}$$

where K_w is assumed to be the same for all of the steps in the proposed model.

The material balance for catalytic reactions is given as follows

$$\frac{dF_i}{dl} = \Omega \cdot \Sigma v_i r_i (1 - \varepsilon) \tag{36}$$

The material balance for noncatalytic reactions is given as follows

$$\frac{dF_i}{dl} = \Omega \cdot \Sigma v_i r_i \varepsilon \tag{37}$$

The heat balance and momentum balance are described as follows

$$\frac{dT}{dl} = \frac{\Sigma(dF_i/dl) \cdot \Delta H_{fi}}{C_{pcat} \cdot F_{cat} + \Sigma C_{pi} \cdot F_i} \tag{38}$$

$$\frac{dP}{dl} = (\rho_p(1 - \varepsilon) + \rho_g \varepsilon)g \tag{39}$$

4.4. Deactivation Model. The effect of coke on the MTO process is complicated, which can be explained by two mechanisms: pore blockage and active site coverage.[78] In the initial period of the MTO reaction, an increase in the coke content does not reduce the total conversion rate but can strengthen the shape selection effect of the catalyst so that the yield of lower olefins increases.[79] Moreover, a sudden decrease in methanol conversion and product yield is observed when the coke content exceeds a certain value, which depends on the properties of the catalyst.[39] Empirical deactivation correlations proposed by Froment[80] cannot reproduce the rapid decrease in catalyst activity. In this case, a specialized model of the SAPO-34 catalyst in the MTO process is necessary. The deactivation model[39] is shown as follows

$$\Phi_i = \frac{1}{1 + 9 \exp(2(w - w_c))} \exp(-a_i w) \tag{40}$$

where w_c is the critical coke content, the value of which depends on the properties of the catalyst and is determined to be 7.0 in eq 40; the preexponential part stands for the abrupt decreasing trend of catalyst activity when the coke content exceeds the critical coke content, while the exponential part is used to represent the selective deactivation. a_i is a function of temperature and has different values for reactions. The relationship between a_i and temperature is re-estimated in this paper.

Considering the activity difference between the circulating spent catalyst and the regenerated catalyst, the catalytic reactions occurring on these two kinds of catalysts are calculated respectively, referring to the parallel compartment (PC) model.[81,82] Note that the catalyst is totally mixed when calculating the hydrodynamic model, but the ratio of the spent catalyst and the regenerated catalyst stays the same at any height. Meanwhile, gaseous components are treated as the homogeneous phase.

In the SMTO process, part of the spent catalyst in the outlet of the reactor is transferred back to its inlet, so iteration calculation is needed to determine the coke content of the spent catalyst, as the value is unknown at the beginning of the simulation. A diagram of the predictive calculation is shown in Figure 4, where $Coke_1$ denotes the coke content on the spent catalyst, and $Coke_2$ denotes the coke content on the regenerated catalyst.

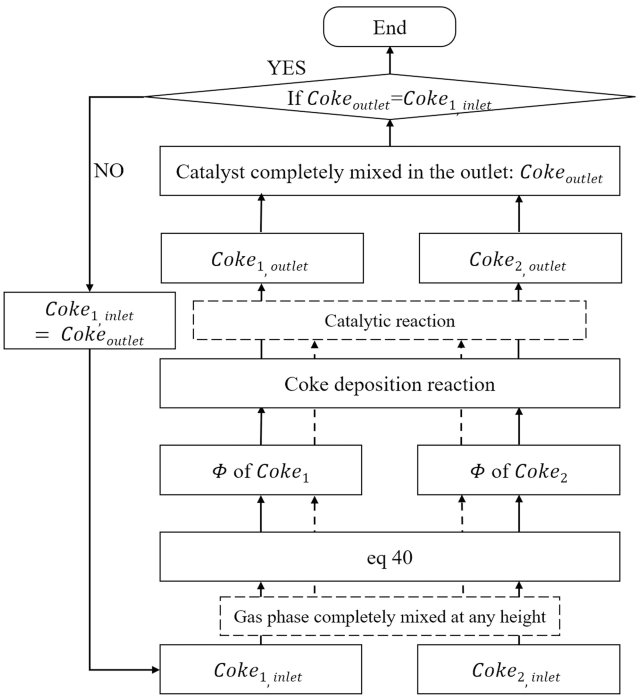

Figure 4. Diagram of the predictive calculation.

5. PARAMETER ESTIMATION

Twenty-four sets of collected industrial data were used to estimate kinetic parameters of the above mathematical model. In this paper, differential equations of the reactor model were solved by the LSODA method,[83] which proves to be more economical than the Runge−Kutta[84] method in most cases. Kinetic parameters were estimated by the COBYLA method. The objective function is the sum of squares of the relative

https://doi.org/10.1021/acsomega.3c00304
ACS Omega 2023, 8, 9630−9643

deviation between the calculated and actual values of the industrial MTO unit, which is shown in eq 41.

$$\text{obj} = \sum_{i}^{m}\sum_{j}^{n}((\text{cal\_value}_{i,j} - \text{act\_value}_{i,j})/\text{act\_value}_{i,j})^2 \quad (41)$$

The estimated results are listed in Tables 4 and 5. The value of K_w is estimated to be 1.7133.

Table 4. Preexponential Factors and Activation Energies

reaction	k_0 (kmol/(m^3·h·MPa^n))	Ea (kJ/kmol)
0	8.92×10^8	5.75×10^4
1	6.82×10^9	7.90×10^4
2	5.40×10^9	7.80×10^4
3	9.13×10^8	7.01×10^4
4	6.39×10^8	6.46×10^4
5	5.78×10^6	8.42×10^4
6	5.40×10^9	7.56×10^4
7	1.01×10^7	7.36×10^4
8	5.93×10^8	7.70×10^4
9	6.23×10^{15}	7.73×10^4
10	2.87×10^8	9.80×10^4
11	3.65×10^7	7.20×10^4
12	1.19×10^6	9.39×10^4
13	9.64×10^7	4.95×10^4
14	7.13×10^{10}	1.16×10^5

Table 5. Relationship between *a* and Temperature

reaction	*a*
1	$-1.20 \times 10^{-5} \times T^2 + 1.79 \times 10^{-2} \times T - 6.63$
2	$-1.35 \times 10^{-5} \times T^2 + 2.05 \times 10^{-2} \times T - 0.77$
3	$-8.97 \times 10^{-5} \times T^2 + 1.36 \times 10^{-1} \times T - 50.6$
4	$-3.10 \times 10^{-7} \times T^2 - 2.81 \times 10^{-3} \times T + 3.36$
5	$-4.20 \times 10^{-5} \times T^2 + 6.21 \times 10^{-2} \times T - 22.9$
6	$-2.18 \times 10^{-5} \times T^2 + 3.17 \times 10^{-2} \times T - 10.5$

Activation energies of reactions range from 50 to 150 kJ/mol. Among the primary reactions, the formation activation energies of CH_4, ethylene, propylene, C_4, and C_5^+ decrease in turn, which is the same as the trend reported in the literature.[34,85] The activation energy of C_5^+ formation is greater than that of C_4 or propylene in other studies.[39,40,86] As the C_5^+ concentration in MTO products is limited, this difference is acceptable. Moreover, the activation energies of secondary reactions are usually greater than those of primary reactions. These phenomena indicate that high temperature is not only favorable for the formation of the main product ethylene, but it also promotes the formation of byproducts, such as CH_4 and coke. As for the formation reactions of ethane, CO, and CO_2, their concentrations in products are limited, and kinetic studies on their formation in the MTO reaction system are rarely reported in the open literature. Therefore, these kinetic parameters are only applicable under SMTO operating conditions. The activity coefficient can be calculated based on eq 40 and Table 5, and its value is inversely proportional to the carbon number of the products, reflecting the influence of the catalyst topology on selectivity.

6. SIMULATION RESULTS

6.1. Model Validation. Model validation was carried out by simulating six sets of commercial data of the SMTO unit under different operating conditions and feedstock compositions. Figure 5 illustrates a comparison between the actual and predicted product distributions of the MTO reactor. The temperature of the reactor outlet was simulated, and it is compared in Figure 6 at the same time. As shown in Figures 5 and 6, data points on both sides of the parity plot's diagonal present good agreement.

6.2. Axial Distribution. The axial distribution of gaseous components, coke content, temperature, and pressure can be strictly calculated by reaction and deactivation kinetics combined with the hydrodynamic model of a fast fluidized bed reactor. A typical set of data from the MTO unit in stable operation is selected for simulation. Table 6 illustrates the operating conditions of the unit. The axial distribution of the main products, pressure, temperature, and voidage are obtained, which are shown in Figures 7−10.

Along the height of the reactor, the main reaction has almost completed in the lower part of the fast fluidized bed because the MTO reaction is rapid and both the catalyst holdup and reactant concentration are high in the lower part of the reactor. The main products decrease in the upper part of the reactor due to side reactions. Thus, the temperature increased and the pressure decreased rapidly within 2 m. This is consistent with industrial data, showing that the temperature in the middle of the reactor is almost the same as that in the upper part. The pressure drop is mainly due to the pressure loss caused by lifting of the catalyst. As the catalyst becomes sparse in the upper part of the fast fluidized bed, the pressure drop also decreases.

6.3. Sensitivity Analysis. The reactor inlet temperature, reactor inlet pressure, coke content, methanol content in the feed, and total feed flow rate are usually the main factors influencing the reaction results. The operating conditions adopted for prediction are the same as those in Table 6. When one of the operating variables was analyzed, the other operating variables remained unchanged during the simulation. The effects of the operating conditions on the reaction are displayed as follows (Figures 11−21).

According to Figure 11, methanol can be completely converted when the inlet temperature ranges from 400 to 500 °C. As the temperature increased, the concentration of ethylene increased while the concentration of butene decreased, and the concentration of propylene first increased and then decreased. This reflects a relatively high activation energy of methanol to ethylene. In this way, temperature is an important tool to regulate the proportion of lower olefins. Increasing the temperature also resulted in more byproducts as well as a higher coke content, as shown in Figure 12. Consequently, either a very high or a very low temperature is not conducive to the selectivity of low-carbon olefins.

The coke content of the inlet catalyst is another key operating condition for plants to adjust the distribution of products besides temperature, which is influenced by the coke content of the spent catalyst. As shown in Figure 13, the selectivity of lower olefins first increased and then decreased. When the coke content of the spent catalyst is greater than 6%, the activity of the catalyst decreases rapidly with an increase in the coke content, leading to an abrupt increase in unconverted reactants and a drastic decrease in main products. These

https://doi.org/10.1021/acsomega.3c00304
ACS Omega 2023, 8, 9630−9643

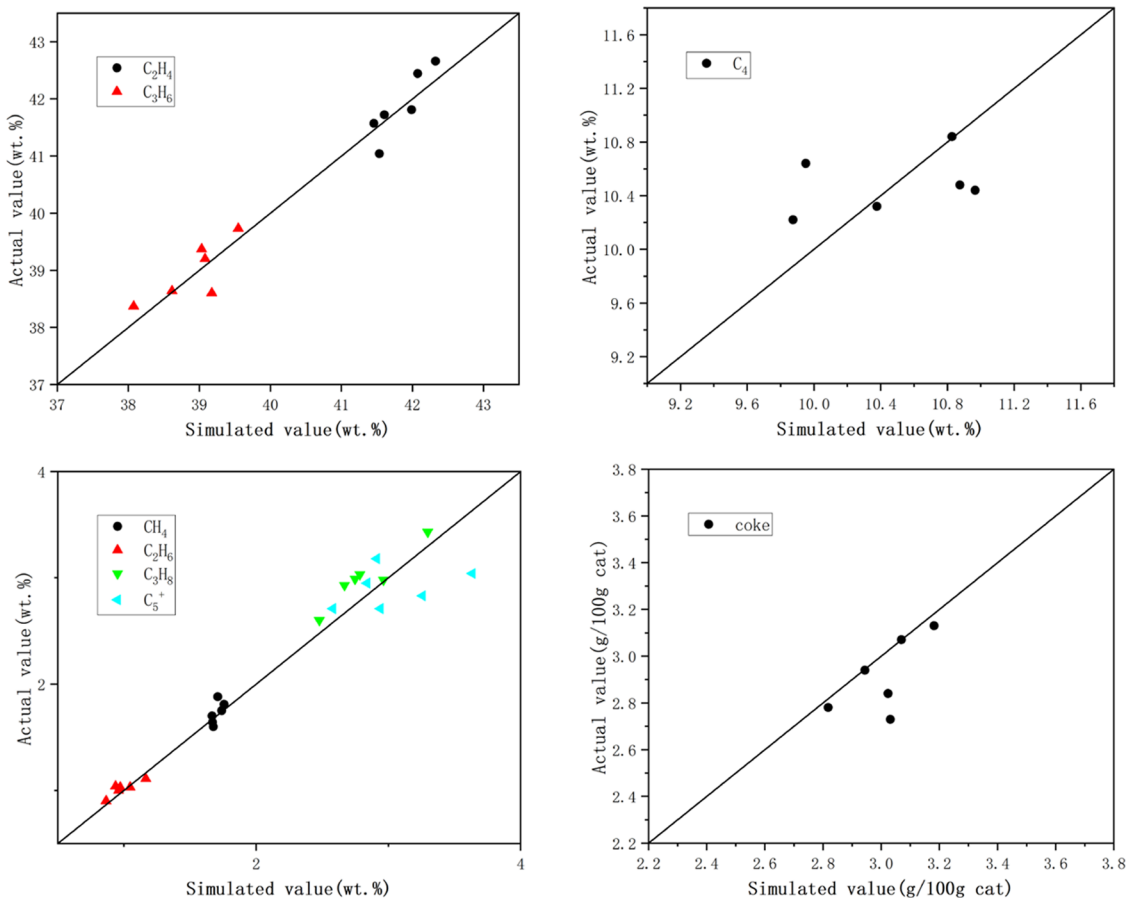

Figure 5. Parity plots for various lump species.

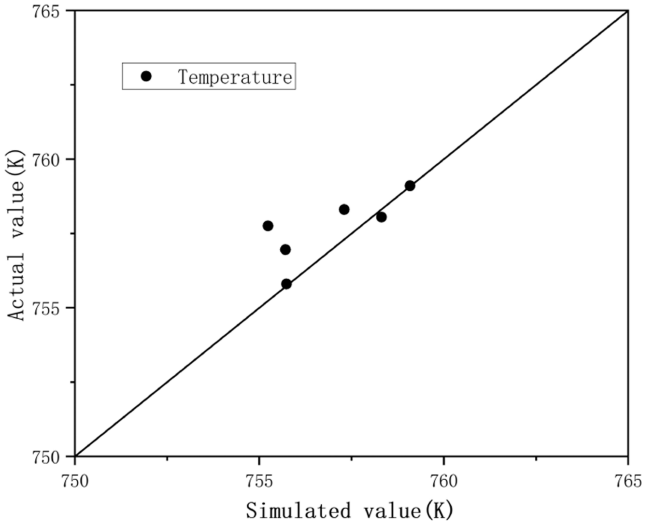

Figure 6. Parity plots for temperature.

phenomena are consistent with the content mentioned in Section 4.4, which proves the applicability of the coke deactivation model.

As shown in Figure 15, the coke content increases with an increase in the inlet pressure due to an increase in the partial pressure of reactants. As for the distribution of the outlet dry gas, which is shown in Figure 14, when the inlet pressure is less than 0.240 MPa, the concentration of unconverted reactants decreases rapidly as the pressure decreases. Low pressure leads to a short residence time of reactants, causing incomplete conversion of methanol. When the inlet pressure is greater than 0.240 MPa, the selectivities of ethylene and propylene slightly decrease because the residence time of reactants in the reactor becomes longer, and ethylene and propylene undergo secondary reactions to form byproducts. The trend of coke is similar to that of ethylene and propylene because coke is the product of primary reactions from reactants (Figure 15). In Figure 16, the catalyst holdup decreases with a decrease in pressure, so the lack of catalyst is a factor that slows down the conversion of reactants under a low inlet pressure.

The effect of the total feed flow rate is similar to that of pressure, which is shown in Figures 17−19. When the total feed flow rate is greater than 220 t/h, the superficial velocity of gas increases with its increase, leading to a decrease in

Table 6. Operating Conditions of the SMTO Unit

conditions	values
inlet temperature (K)	703.71
inlet pressure (Pa)	251 735
inlet coke content of spent catalyst (g/100 g·catalyst)	3.07
inlet coke content of regenerated catalyst (g/100 g·catalyst)	0.19
feed flow rate (t/h)	201.77
methanol content (wt %)	95.25
water content (wt %)	4.37
higher alcohols (wt %)	0.38
dilute steam (t/h)	18.52
spent catalyst flow rate (t/h)	3023.13
regenerated catalyst flow rate (t/h)	138.38

https://doi.org/10.1021/acsomega.3c00304
ACS Omega 2023, 8, 9630−9643

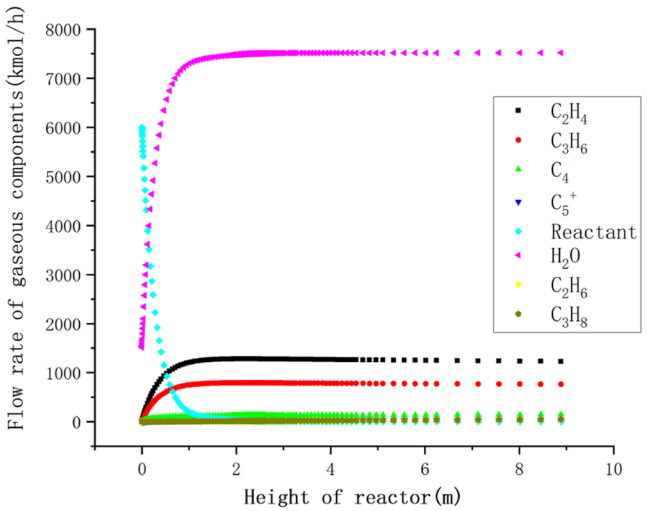

Figure 7. Axial distribution of main products.

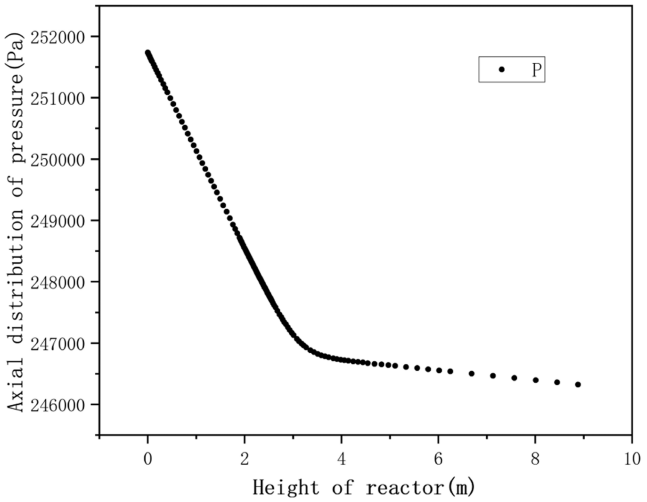

Figure 8. Axial distribution of pressure.

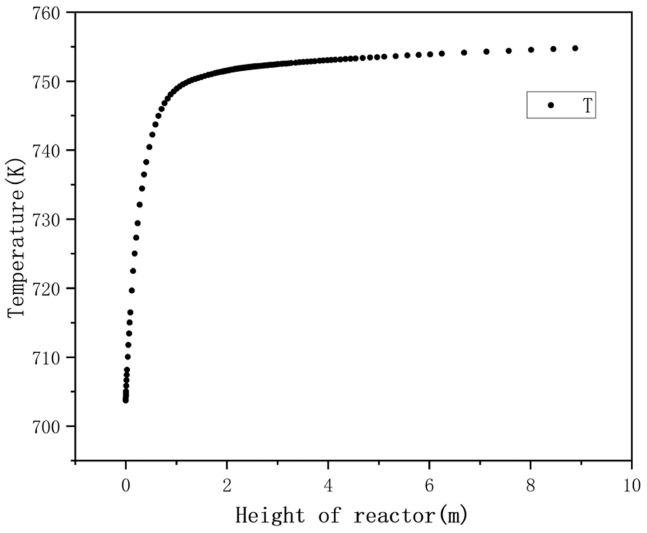

Figure 9. Axial distribution of temperature.

residence time. Consequently, reactions cannot complete in such a short residence time. In contrast, when the total feed flow rate is less than 220 t/h, the main reactions are completed

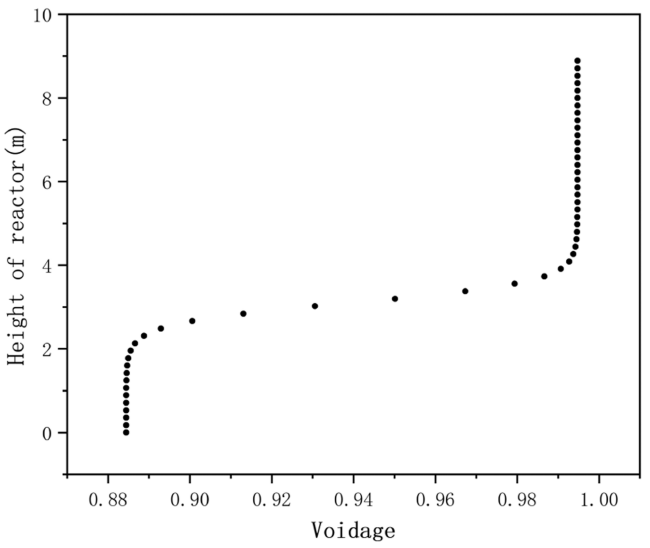

Figure 10. Axial distribution of voidage of the reactor.

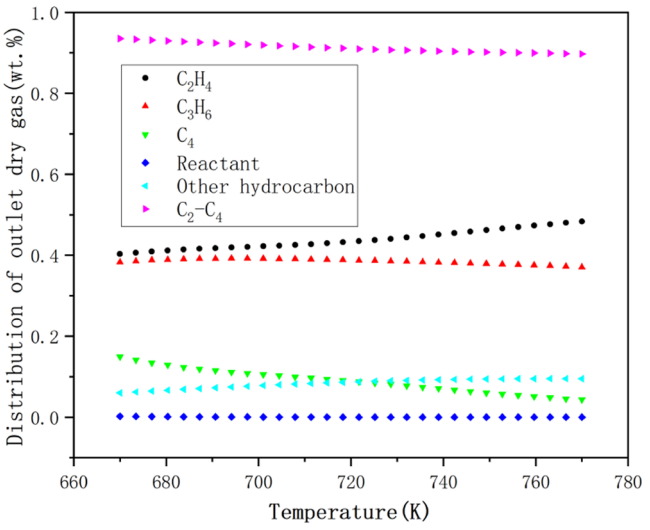

Figure 11. Distribution of outlet dry gas versus temperature.

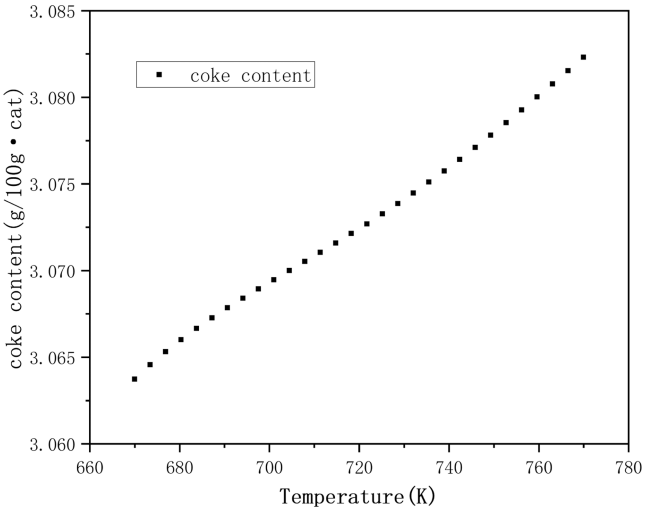

Figure 12. Coke content of the outlet versus temperature.

https://doi.org/10.1021/acsomega.3c00304
ACS Omega 2023, 8, 9630−9643

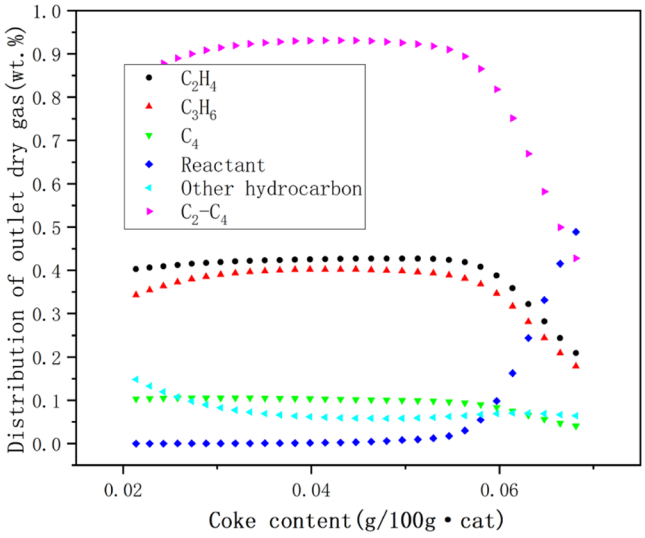

Figure 13. Distribution of outlet dry gas versus coke content.

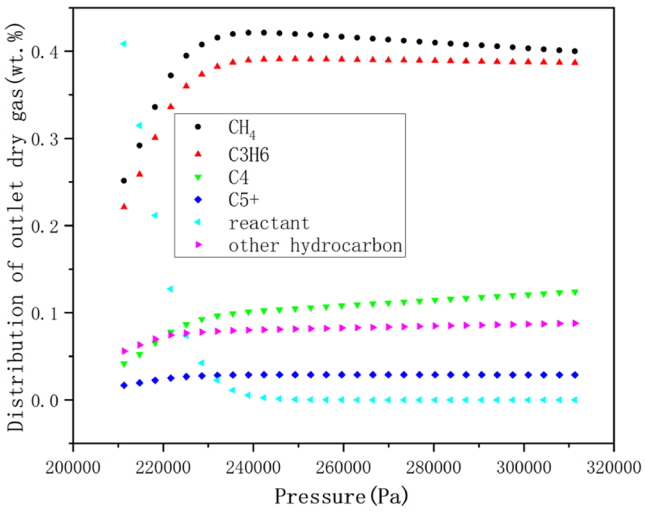

Figure 14. Distribution of outlet dry gas versus pressure.

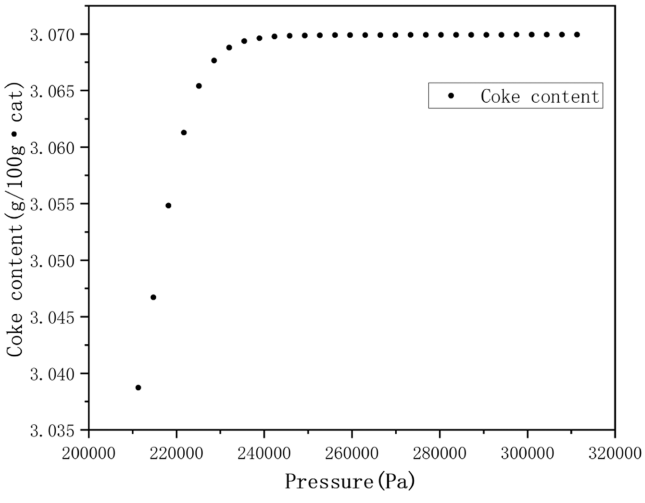

Figure 15. Coke content of outlet versus pressure.

in advance, leading to an increase in byproducts. The catalyst holdup decreases with an increase in the total feed flow rate, which slows down the reaction rate.

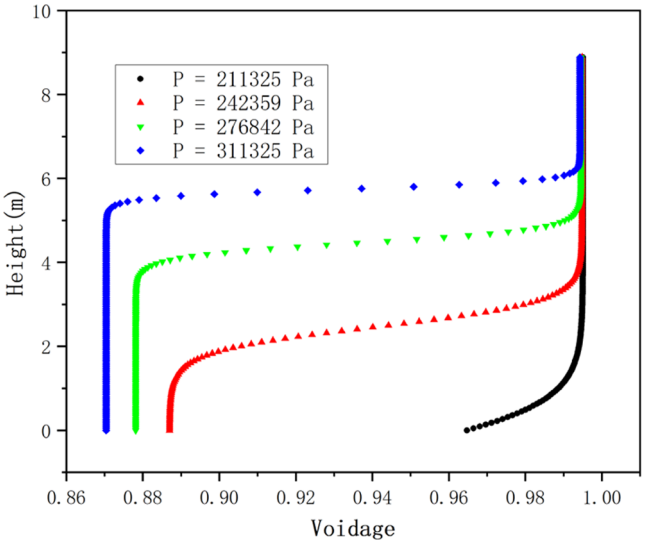

Figure 16. Effect of pressure on axial voidage.

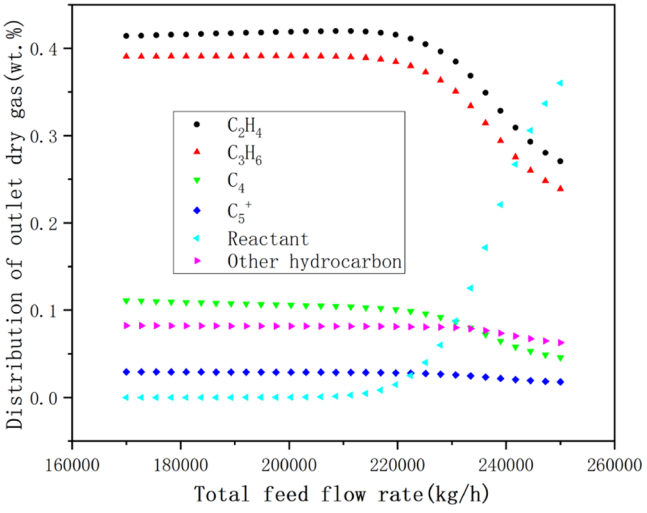

Figure 17. Distribution of outlet dry gas versus total flow rate.

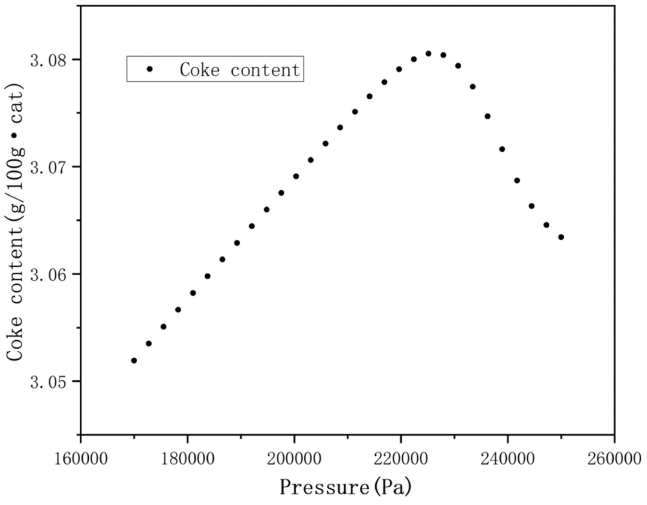

Figure 18. Coke content of outlet versus total feed flow rate.

According to Figures 20 and 21, when the methanol content is less than about 0.8, the reaction rate decreases rapidly, and

https://doi.org/10.1021/acsomega.3c00304
ACS Omega 2023, 8, 9630−9643

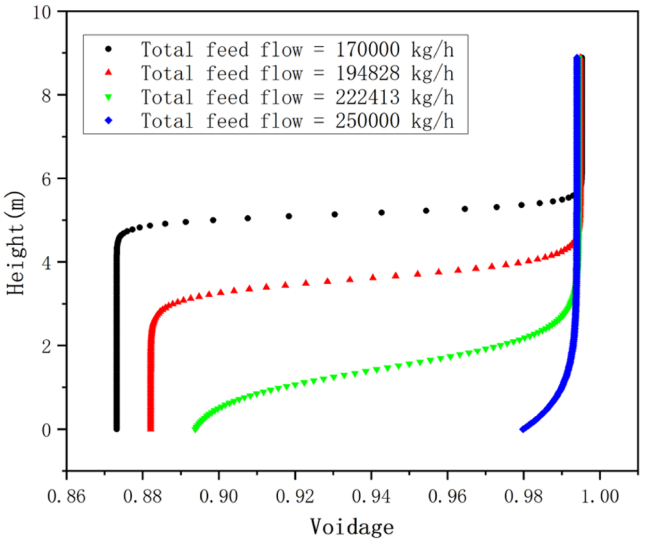

Figure 19. Effect of total feed flow rate on axial voidage.

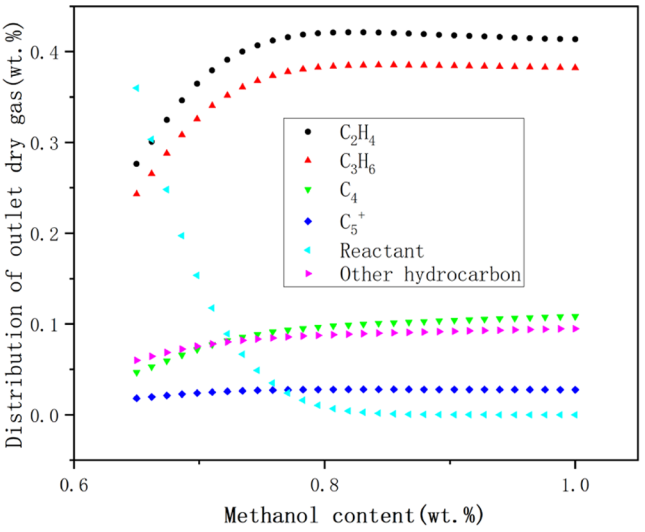

Figure 20. Distribution of outlet dry gas versus methanol content.

coke deposition slows down with a decrease in methanol, which can be attributed to the low partial pressure of methanol and competitive adsorption of water against methanol. However, methanol content has little impact on olefin selectivity.

In conclusion, the temperature and the catalyst coke content are the main operating conditions affecting the product yield and reactant conversion rate. However, the pressure, total feed flow rate, and methanol content affect the reactant conversion rate but have little effect on the yield.

7. CONCLUSIONS

A reaction kinetic model with 15 reactions and 14 lumps, combined with a fast fluidized bed reactor model, was established based on the data from the industrial SMTO process, considering the activity difference between the circulating spent catalyst and the regenerated catalyst. The validation results showed a good fit to the actual industrial data, and the sensitivity analysis results showed the effect of the main operation variables on reaction conversion and product distribution, which can provide quantitative guidance for optimizing the operation of an industrial SMTO reactor.

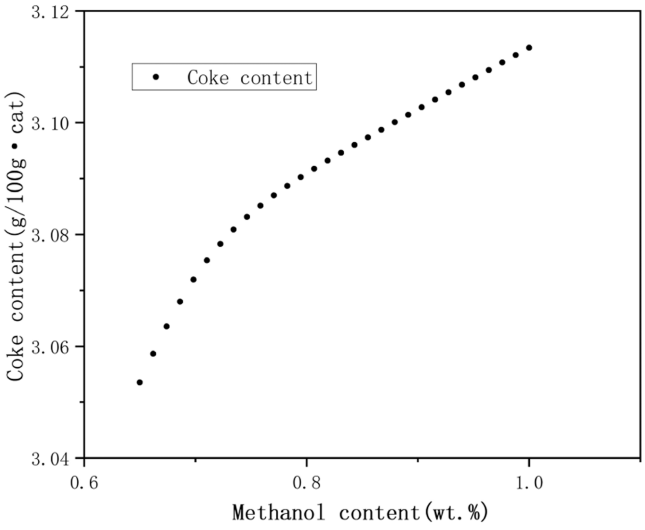

Figure 21. Coke content of outlet versus methanol content.

AUTHOR INFORMATION

Corresponding Author

Hongbo Jiang − *Research Institute of Petroleum Processing, East China University of Science and Technology, Shanghai 200237, China;* orcid.org/0000-0002-3025-682X; Phone: 86-21-64252816; Email: hbjiang@ecust.edu.cn

Authors

Linzhi Yuan − *Research Institute of Petroleum Processing, East China University of Science and Technology, Shanghai 200237, China*

Defei Li − *Petro-CyberWorks Information Technology Co., Ltd., Shanghai 200050, China*

Yushi Chen − *Petro-CyberWorks Information Technology Co., Ltd., Shanghai 200050, China*

Complete contact information is available at: https://pubs.acs.org/10.1021/acsomega.3c00304

Notes

The authors declare no competing financial interest.

NOTATIONS

Ar	Archimedes number
a_i	deactivation fitting parameter of reaction i
act_value$_{i,j}$	actual values
C_{pcat}	heat capacity of catalyst, kJ/kg
C_{pi}	heat capacity of lump i, kJ/kmol
cal_value$_{i,j}$	calculated values
D	diameter of reactor, m
d_p	particle diameter, m
Ea$_i$	activation energy of reaction i, J/mol
F_i	flow rate of lump i, kmol/h
F_{cat}	flow rate of catalyst, kg/h
g	gravitational constant, 9.8 kg/N
G_s	solid mass flux, kg/(m^2·s)
G_{sm}	minimum solid mass flux, kg/(m^2·s)
G_s^*	saturation carrying capacity of gas, kg/(m^2·s)
H	water effect parameter
k	rate constants of reaction i, kmol/(m^3·h·MPa^n)

https://doi.org/10.1021/acsomega.3c00304
ACS Omega 2023, 8, 9630−9643

k_i	preexponential factor of reaction i, kmol/(m^3·h·MPa^n)
K_i	standard equilibrium constant of reaction i
K_w	resistance constant
l	length of reactor, m
m	set number of commercial operational data
n	number of lumps
P_i	partial pressure of lump i, MPa
P	pressure, Pa
R	universal gas constant, kJ/mol
r_i	reaction rate, kmol/(m^3·h)
T	temperature, K
u_c	minimum fast point velocity, m/s
u_d	superficial solid velocity, m/s
u_g	superficial gas velocity, m/s
u_{pt}	onset superficial gas velocity for fast fluidization, m/s
v_i	stoichiometric number
w	coke content, g/100g·cat
w_c	critical coke content, g/100g·cat
X_w	molar fraction of water
Z_0	characteristic height, m
Z_i	height of the point between the inflection dilute phase and two dense phases, m
ε	voidage in the fast fluidized bed
ε_d	voidage at the bottom of the fast fluidized bed
ε_e	voidage at the top of the fast fluidized bed
ε^*	limiting voidage of dilute phase
γ	decay constant
μ	gas viscosity, kg/m s
ϕ_i	deactivation function of reaction i
ρ_g	gas density, kg/m^3
ρ_p	particle density, kg/m^3
Ω	cross-sectional area of reactor, m^2
ΔH_{fi}	enthalpy of formation of reaction i

REFERENCES

(1) Liu, S.; Yang, L.; Chen, B.; Yang, S.; Qian, Y. Comprehensive energy analysis and integration of coal-based MTO process. *Energy* **2021**, *214*, No. 119060.

(2) Standl, S.; Hinrichsen, O. Kinetic Modeling of Catalytic Olefin Cracking and Methanol-to-Olefins (MTO) over Zeolites: A Review. *Catalysts* **2018**, *8*, 626.

(3) Aitani, A.; Yoshikawa, T.; Ino, T. Maximization of FCC light olefins by high severity operation and ZSM-5 addition. *Catal. Today* **2000**, *60*, 111−117.

(4) Cavani, F.; Trifirò, F. The oxidative dehydrogenation of ethane and propane as an alternative way for the production of light olefins. *Catal. Today* **1995**, *24*, 307−313.

(5) Jiang, G.; Li, Z.; Zhen, Z.; Zhou, X.; Gao, J.; et al. Highly effective P-modified HZSM-5 catalyst for the cracking of C4 alkanes to produce light olefins. *Appl. Catal., A* **2008**, *340*, 176−182.

(6) Tian, P.; Wei, Y.; Ye, M.; Liu, Z. Methanol to Olefins (MTO): From Fundamentals to Commercialization. *ACS Catal* **2015**, *5*, 1922−1938.

(7) Sarp, S.; Gonzalez Hernandez, S.; Chen, C.; Sheehan, S. W. Alcohol Production from Carbon Dioxide: Methanol as a Fuel and Chemical Feedstock. *Joule* **2021**, *5*, 59−76.

(8) Duan, M. Z.; Jiang, L. F.; Zhang, Z. G.; Zheng, H. A. Research Progress on Methanol to Olefins Fluidized Bed Reactor. *Guangzhou Chem. Ind.* **2016**, *44*, 3.

(9) Jiang, Y. Z.; Yang, Y. F.; Wei, X. F.; Li, G. F. Latest progress in methanol to olefin process and industrialization. *Nat. Gas Chem. Ind.* **2020**, *45*, 6.

(10) Nan, H. M.; Wen, Y. S.; Wu, X. Z.; Xu, C. M.; Guan, F. Z.; G, L. Recent development of methanol to olefins technology. *Mod. Chem. Ind.* **2014**, 6.

(11) Zhang, S. J.; Wu, X. Z.; Liu, Y.; Ji, G. C.; Wen, Y. S. Latest progress of methanol to olefin process and industrialization. *Mod. Chem. Ind.* **2017**, *37*, 6.

(12) Liang, J.; Li, H.; Zhao, S.; Guo, W.; Wang, R.; Ying, M. Characteristics and performance of SAPO-34 catalyst for methanol-to-olefin conversion. *Appl. Catal.* **1990**, *64*, 31−40.

(13) Wu, X. Z. Methanol to Lower Olefins. In *Coal to Low Carbon Olefin Process and Engineering*, Wu, X. Z., Ed.; Academic Press: Chemical Industry Press Co., Ltd., 2014; pp 272−452.

(14) Wright, P. A.; Pearce, G. M. Structural Chemistry of Zeolites. In *Zeolites and Catalysis*, Jiři Čejka, A. C.; Stacey, Z., Eds.; Wiley-VCH Verlag GmbH & Co. KGaA, 2010; pp 171−207.

(15) Dahl, I. M.; Kolboe, S. On the reaction mechanism for propene formation in the MTO reaction over SAPO-34. *Catal. Lett.* **1993**, *20*, 329−336.

(16) Dahl, I. M.; Kolboe, S. On the Reaction Mechanism for Hydrocarbon Formation from Methanol over SAPO-34: I. Isotopic Labeling Studies of the Co-Reaction of Ethene and Methanol. *J. Catal.* **1994**, *149*, 458−464.

(17) Dahl, I. M.; Kolboe, S. On the Reaction Mechanism for Hydrocarbon Formation from Methanol over SAPO-34: 2. Isotopic Labeling Studies of the Co-reaction of Propene and Methanol. *J. Catal.* **1996**, *161*, 304−309.

(18) Svelle, S.; Joensen, F.; Nerlov, J.; Olsbye, U.; Lillerud, K. P.; Kolboe, S.; Bjørgen, M. Conversion of Methanol into Hydrocarbons over Zeolite H-ZSM-5: Ethene Formation Is Mechanistically Separated from the Formation of Higher Alkenes. *J. Am. Chem. Soc.* **2006**, *128*, 14770.

(19) Bjørgen, M.; Svelle, S.; Joensen, F.; Nerlov, J.; Kolboe, S.; Bonino, F.; Palumbo, L.; Bordiga, S.; Olsbye, U. Conversion of methanol to hydrocarbons over zeolite H-ZSM-5: On the origin of the olefinic species. *J. Catal.* **2007**, *249*, 195−207.

(20) Yuan, X. X.; Li, H.; Ye, M.; Liu, Z. M. Kinetic modeling of methanol to olefins process over SAPO-34 catalyst based on the dual-cycle reaction mechanism. *AIChE J.* **2019**, *65*, 662−674.

(21) Dai, W. L.; Wang, C. M.; Dyballa, M.; Wu, G. J.; Guan, N. J.; Li, L. D.; Xie, Z. K.; Hunger, M. Understanding the Early Stages of the Methanol-to-Olefin Conversion on H-SAPO-34. *ACS Catal.* **2015**, *5*, 317−326.

(22) Mole, T.; Whiteside, J.A. Conversion of methanol to ethylene over ZSM-5 zeolite in the presence of deuterated water. *J. Catal.* **1982**, *75*, 284−290.

(23) Sassi, A.; Wildman, M. A.; Ahn, H. J.; Prasad, P.; Nicholas, J. B.; Haw, J. F. Methylbenzene Chemistry on Zeolite HBeta: Multiple Insights into Methanol-to-Olefin Catalysis. *J. Phys. Chem. B* **2002**, *106*, 2294−2303.

(24) Haw, J. F.; Song, W.; Marcus, D. M.; Nicholas, J. B. The Mechanism of Methanol to Hydrocarbon Catalysis. *Acc. Chem. Res.* **2003**, *36*, 317−326.

(25) Lesthaeghe, D.; Horr, A.; Waroquier, M., Dr.; Marin, G. B., Dr.; Van Speybroeck, V., Dr. Theoretical Insights on Methylbenzene Side-Chain Growth in ZSM-5 Zeolites for Methanol-to-Olefin Conversion. *Chem. - Eur. J.* **2009**, *15*, 10803−10808.

(26) Kumar, P.; Thybaut, J. W.; Svelle, S.; Olsbye, U.; Marin, G. B. Single-event microkinetics for methanol to olefins on H-ZSM-5. *Ind. Eng. Chem. Res.* **2013**, *52*, 1491−1507.

(27) Mihail, R.; Straja, S.; Maria, G.; Musca, G.; Pop, G. Kinetic model for methanol conversion to olefins. *Ind. Eng. Chem. Process Des. Dev.* **1983**, *22*, 532−538.

(28) Bos, A. N. R.; Tromp, P.; Akse, H. N. Conversion of Methanol to Lower Olefins. Kinetic Modeling, Reactor Simulation, and Selection. *Ind. Eng. Chem. Res.* **1995**, *34*, 134−135.

(29) Gayubo, A. G.; Aguayo, A. T.; Campo, A.; Tarrio, A. M.; Bilbao, J. Kinetic Modeling of Methanol Transformation into Olefins on a SAPO-34 Catalyst. *Ind. Eng. Chem. Res.* **2000**, *39*, 292−300.

https://doi.org/10.1021/acsomega.3c00304
ACS Omega 2023, 8, 9630−9643

(30) Park, T. Y.; Froment, G. F. Kinetic Modeling of the Methanol to Olefins Process. 1. Model Formulation. *Ind. Eng. Chem. Res.* **2001**, *40*, 4172−4186.
(31) Park, T. Y.; Froment, G. F. Kinetic Modeling of the Methanol to Olefins Process. 2. Experimental Results, Model Discrimination, and Parameter Estimation. *Ind. Eng. Chem. Res.* **2001**, *40*, 4187−4196.
(32) Alwahabi, S. M.; Froment, G. F. Single Event Kinetic Modeling of the Methanol-to-Olefins Process on SAPO-34. *Ind. Eng. Chem. Res.* **2004**, *43*, 772−772.
(33) Qi, G. Z.; Ma, T.; Liu, H. X.; Xie, Z. K.; Zhang, C. F.; Chen, Q. L. Kinetics of methanol to olefins. *Chin. J. Chem. Eng.* **2005**, *56*, 6.
(34) Qi, G. Z. A Study on the Process of Methanol to Olefins Reaction, Ph.D. Thesis. East China University of Science and Technology: Shanghai, China, 2006.
(35) Chen, D.; Grønvold, A.; Moljord, K.; Holmen, A. Methanol Conversion to Light Olefins over SAPO-34: Reaction Network and Deactivation Kinetics. *Ind. Eng. Chem. Res.* **2007**, *46*, 4116−4123.
(36) Hu, H.; Ying, W.; Fang, D. Mathematical modeling of multi-bed adiabatic reactor for the Methanol-to-Olefin process. *React. Kinet., Mech. Catal.* **2010**, *101*, 49−61.
(37) Hu, H. Research of Catalytic Reaction Engineering for Methanol-to-Olefin Process, Ph.D. Thesis. East China University of Science and Technology: Shanghai, China, 2010.
(38) Sedighi, M.; Bahrami, H.; Towfighi, J. Kinetic modeling formulation of the methanol to olefin process: Parameter estimation. *J. Korean Ind. Eng. Chem.* **2014**, *20*, 3108−3114.
(39) Ying, L.; Lei, Y.; Yuan, X.; Ye, M.; Mao, Y.; Cheng, Y.; Liu, Z. A seven lumped kinetic model for industrial catalyst in DMTO process. *Chem. Eng. Res. Des.* **2015**, *100*, 179−191.
(40) Ying, L. Kinetics of Methanol and Olefins Formation Over SAPO-34 and ZSM-5 catalvst, Ph.D. Thesis. Zhejiang University: Hangzhou, China, 2015.
(41) Ying, L.; Ye, M.; Cheng, Y. W.; Li, X. Characteristics of Coke Deposition Over a SAPO-34 Catalyst in the Methanol-to-Olefins Reaction. *J. Pet. Sci. Technol.* **2015**, *33*, 984−991.
(42) Rostami, R. B.; Lemraski, A. S.; Ghavipour, M.; Behbahani, R. M.; Shahraki, B. H.; Hamule, T. Kinetic modelling of methanol conversion to light olefins process over silicoaluminophosphate (SAPO-34) catalyst. *Chem. Eng. Res. Des.* **2016**, *106*, 347−355.
(43) Li, Y.; Kwauk, M. The Dynamics of Fast Fluidization. In *Fluidization*, Grace, J. R.; Matsen, J. M., Eds.; Springer US: Boston, MA, 1980; pp 537−544.
(44) Kwauk, M.; Ningde, W.; Youchu, L.; Bingyu, C.; Zhiyuan, S. Fast Fluidization at ICM. In *Circulating Fluidized Bed Technology*, Basu, P., Ed.; Pergamon: Oxford, 1986; pp 33−62.
(45) Li, J. H. Multi-scale Modeling and Method of Energy Minimization in Two-phase Flow, Ph.D. ThesisChinese Academy of Sciences: Beijing, China, 1987.
(46) Li, J.; Tung, Y.; Kwauk, M. Energy Transport and Regime Transition in Particle-Fluid Two-Phase Flow. In *Circulating Fluidized Bed Technology*, 1988; pp 75−87.
(47) Li, J.; Tung, Y.; Kwauk, M. Method of Energy Minimization in Multi-scale Modeling of Particle Fluid Two-phase Flow. In *Circulating Fluidized Bed Technology*, 1988; pp 89−103.
(48) Li, J.; Tung, Y.; Kwauk, M. Axial Voidage Profiles of Fast Fluidized Beds in Different Operating Regions. In *Circulating Fluidized Bed Technology*, Basu, P.; Large, J. F., Eds.; Pergamon, 1988; pp 193−203.
(49) Li, J.; Reh, L.; Kwauk, M. Application of the Principle of Energy Minimization to the Fluid Dynamics of Circulating Fluidized Beds. In *Circulating Fluidized Bed Technology III*, Pergamon Press: Oxford, 1990; 105−111.
(50) Bai, D.; Zhu, J. X.; Jin, Y.; Yu, Z. Internal recirculation flow structure in vertical upflow gas-solids suspensions Part I. A core-annulus model. *Powder Technol.* **1995**, *85*, 171−177.
(51) Bai, D.; Zhu, J. X.; Jin, Y.; Yu, Z. Internal recirculation flow structure in vertical upflow gas-solid suspensions Part II. Flow structure predictions. *Powder Technol.* **1995**, *85*, 179−188.
(52) Thompson, M. L.; Bi, H.; Grace, J. R. A generalized bubbling/turbulent fluidized-bed reactor model. *Chem. Eng. Sci.* **1999**, *54*, 2175−2185.
(53) Abba, I. A.; Grace, J. R.; Bi, H. T.; Thompson, M. L. Spanning the flow regimes: Generic fluidized-bed reactor model. *AIChE J.* **2003**, *49*, 1838−1848.
(54) Constantineau, J. P.; Grace, J. R.; Lim, C. J.; Richards, G. G. Generalized bubbling−slugging fluidized bed reactor model. *Chem. Eng. Sci.* **2007**, *62*, 70−81.
(55) Kunii, D.; Levenspiel, O.; Brenner, H. *Fluidization Engineering*, 2nd ed.; Elsevier Inc.: Boston, 1991.
(56) Zheng, K. Simulation of Methanol to Olefins (MTO) Fluidized Bed Reactor. Ph.D. ThesisZhejiang University: Hangzhou, China, 2012.
(57) Bi, X. Gas Fluidization Flow Regimes. *Essentials of Fluidization Technology*, 2020; 55−74.
(58) Chen, B. Y.; Li, Y. C.; Wang, F. M.; Wang, Y. S.; Guo, M. S. Study on Fast Fluidization (II) Formation Conditions of Fast Fluidized Bed and Its Prediction. *Chin. J. Process Eng.* **1980**, 32−40.
(59) Bi, X. T.; Jin, Y. The Criterion of Transition from Fast Fluidization to Peneumatic Transport. *Chin. J. Chem. Eng.* **1990**, *41*, 623−625.
(60) Li, Y. C.; Chen, B. Y.; Wang, F. M.; Wang, Y. S.; Guo, M. S. Study on Fast Fluidization (I) Parameter Correlation of Fast Fluidization Hydrodynamic Model. *Chin. J. Process Eng.* **1980**, 22−32.
(61) Bai, D.; Kato, K. Quantitative estimation of solids holdups at dense and dilute regions of circulating fluidized beds. *Powder Technol.* **1999**, *101*, 183−190.
(62) Adánez, J.; Gayán, P.; García-Labiano, F.; de Diego, L. F. Axial voidage profiles in fast fluidized beds. *Powder Technol.* **1994**, *81*, 259−268.
(63) Chang, C. D.; Silvestri, A. J. The conversion of methanol and other O-compounds to hydrocarbons over zeolite catalysts. *J. Catal.* **1977**, *47*, 249−259.
(64) Chang, C. D. Hydrocarbons from Methanol. *Catal. Rev.* **1983**, *25*, 1−118.
(65) Swabb, E. A.; Gates, B. C. Diffusion, Reaction, and Fouling in H-Mordenite Crystallites. The Catalytic Dehydration of Methanol. *Ind. Eng. Chem. Fundam.* **1972**, *11*, 540−545.
(66) Hutchings, G. J.; Gottschalk, F.; Hall, M. V. M.; Hunter, R. Hydrocarbon formation from methylating agents over the zeolite catalyst ZSM-5. Comments on the mechanism of carbon−carbon bond and methane formation. *J. Chem. Soc., Faraday Trans. 1* **1987**, *83*, 571−583.
(67) Olah, G. A. Higher coordinate (hypercarbon containing) carbocations and their role in electrophilic reactions of hydrocarbons. *Pure Appl. Chem.* **1981**, *53*, 201−207.
(68) Ono, Y.; Mori, T. Mechanism of methanol conversion into hydrocarbons over ZSM-5 zeolite. *J. Chem. Soc., Faraday Trans. 1* **1981**, *77*, 2209.
(69) Kagi, D. In re: Mechanism of conversion of methanol over ZSM-5 catalyst. *J. Catal.* **1981**, *69*, 242−243.
(70) Clarke, J. K. A.; Darcy, R.; Hegarty, B. F.; O'Donoghue, E.; Amir-Ebrahimi, V.; Rooney, J. J. Free radicals in dimethyl ether on H-ZSM-5 zeolite. A novel dimension of heterogeneous catalysis. *J. Chem. Soc., Chem. Commun.* **1986**, 425−426.
(71) Dahl, I. M.; Kolboe, S. On the Reaction Mechanism for Hydrocarbon Formation from Methanol over SAPO-34: 2. Isotopic Labeling Studies of the Co-reaction of Propene and Methanol. *J. Catal.* **1996**, *161*, 304−309.
(72) Mole, T.; Bett, G.; Seddon, D. Conversion of Methanol to Hydrocarbons over ZSM-5 Zeolite: An Examination of the Role of Aromatic Hydrocarbons Using 13Carbon and Deuterium Labeled Feeds. *J. Catal.* **1983**, *84*, 435−445.
(73) Mole, T.; Whiteside, J. A.; Seddon, D. Aromatic co-catalysis of methanol conversion over zeolite catalysts. *J. Catal.* **1983**, *82*, 261−266.

https://doi.org/10.1021/acsomega.3c00304
ACS Omega 2023, 8, 9630−9643

(74) Zhou, H. Q.; Wang, Y.; Wei, F.; Wang, D. Z.; Wang, Z. W. Kinetics of the reactions of the light alkenes over SAPO-34. *Appl. Catal., A* **2008**, *348*, 135−141.
(75) Benito, P. L.; Gayubo, A. G.; Aguayo, A. T.; Castilla, M.; Bilbao, J. Concentration-Dependent Kinetic Model for Catalyst Deactivation in the MTG Process. *Ind. Eng. Chem. Res.* **1996**, *35*, 81−89.
(76) Hao, H.; Ying, W.; Fang, D. Reaction and deactivation kinetics of methanol-to-olefins process based on a special TGA reactor. *J. Nat. Gas Chem.* **2010**, *19*, 409−416.
(77) Li, N.; Chen, M.; Liu, D. Deactivation kinetics with activity coefficient of the methanol to aromatics process over modified ZSM-5. *Fuel* **2018**, *233*, 283−290.
(78) Guisnet, M. "Coke" molecules trapped in the micropores of zeolites as active species in hydrocarbon transformations. *J. Mol. Catal. A: Chem.* **2002**, *182−183*, 367−382.
(79) Qi, G. Z.; Xie, Z. K.; Yang, W. M.; Zhong, S. Q.; Chen, Q. L.; et al. Behaviors of coke deposition on SAPO-34 catalyst during methanol conversion to light olefins. *Fuel Process. Technol.* **2007**, *88*, 437−441.
(80) Froment, G. F.; Bischoff, K. B.; Wilde, J. D. *Chemical Reactor Analysis and Design*, 3rd ed.; Elsevier Scientific Pub. Co., 1981.
(81) Cordero-Lanzac, T.; Aguayo, A. T.; Gayubo, A. G.; Bilbao, J. Consideration of the activity distribution using the population balance theory for designing a dual fluidized bed reactor-regenerator system. Application to the MTO process. *Chem. Eng. J.* **2021**, *405*, 126448.
(82) Cordero-Lanzac, T.; Aguayo, A. T.; Gayubo, A. G.; Castaño, P.; Bilbao, J. A comprehensive approach for designing different configurations of isothermal reactors with fast catalyst deactivation. *Chem. Eng. J.* **2020**, *379*, No. 122260.
(83) Petzold, L. Automatic Selection of Methods for Solving Stiff and Nonstiff Systems of Ordinary Differential Equations. *SIAM J. Sci. Stat. Comput.* **1983**, *4*, 136−148.
(84) Tikhonov, A. N.; Gorbunov, A. D. Asymptotic expansions of the error in the difference method of solving Cauchy's problem for systems of differential equations equations. *Comput. Math. Math. Phys.* **1963**, *2*, 565−580.
(85) Pu, J. L. A Study on the Kinetic Model of Methanol to Olefins Reaction Process. M.S. ThesisEast China University of Science and Technology: Shanghai, China, 2014.
(86) Lee, M. K.; Kim, J.; Ryu, J. H.; Yoon, Y. S.; Kim, C. U.; Jeong, S. Y.; Lee, I. B. Modeling of Reaction and Deactivation Kinetics in Methanol-to-Olefins Reaction on SAPO-34. *Ind. Eng. Chem. Process Des. Dev.* **2019**, *58*, 13227.

https://doi.org/10.1021/acsomega.3c00304
ACS Omega 2023, 8, 9630−9643